Preparation of Poly(4-methyl-1-pentene) Asymmetric or Microporous Hollow-Fiber Membranes by Melt-Spun and Cold-Stretch Method

Jianli Wang,[1] Zhikang Xu,[2] Youyi Xu[2]

[1]*Zhejiang Key Laboratory of Green Chemistry Synthesis Technology, College of Chemical Engineering and Materials, Zhejiang University of Technology, 310014, Hangzhou, People's Republic of China*
[2]*Institute of Polymer Science, Zhejiang University, 310027, Hangzhou, People's Republic of China*

Received 6 January 2005; accepted 11 July 2005
DOI 10.1002/app.23597
Published online in Wiley InterScience (www.interscience.wiley.com).

ABSTRACT: Poly(4-methyl-1-pentene) (PMP) hollow fibers were prepared and fabricated into gas separation or microporous membranes by the melt-spun and cold-stretched method. PMP resin was melt-extruded into hollow fibers with cold air as the cooling medium. The effects of take-up speed and thermotreatment on the mechanical behavior and morphology of the fibers were investigated. Scanning electronic microscope (SEM) photos were used to reveal the geometric structure of the section and surface of the hollow fibers. It was found that the original fiber had an asymmetric structure. A "sandwich" mode was used to describe the formation of this special fine structure. And a series of PMP hollow-fiber membranes were prepared by subsequent drawing, and it was found that there was a "skin–core" structure on the cross section of these hollow-fiber membranes. Asymmetric or microporous PMP hollow-fiber membranes could be obtained by controlling posttreatment conditions. The morphology of these membranes were characterized by SEM, and the gas (oxygen, nitrogen, and carbon dioxide) permeation properties of the membranes was measured. The results indicate that the annealing time of the original fiber and the stretching ratio were the key factors influencing the structure of the resulting membrane.
 J Appl Polym Sci 100: 2131–2141, 2006

Key words: polyolefins; membranes; morphology

INTRODUCTION

Semicrystalline polymers such as polypropylene and polyethylene were used for the preparation of microporous membranes by methods including the thermo-induced phase separation (TIPS)[1–4] melt-spun and cold-stretched (MSCS),[5–8] and filling–stretching (FS)[9] methods. Membranes possessing microporous morphologies have found a wide variety of commercial applications in, for example, microfiltration, blood oxygenation, dialysis, reciprocator membranes, and membrane contactors.[10–14] To fabricate such microporous materials, a number of methods have been proposed. These range from the swelling of a semicrystalline material followed by later stretching and removal of the swelling solvent[15,16]; stretching (uniaxially and/or biaxially) of a polymer matrix containing filler particles that have poor adhesion to the matrix, leading to cavitation of the matrix upon deformation;[9,17] to fibrillation by biaxial stretching such as those methods based on polytetrafluroethylene.[18] The melt-spun method is the most economical for hollow-fiber membrane production. It is also a very ecological method, as no wastewater or harmful byproducts are involved. Of all the thermoplastic polymers that can be processed by melt spinning, polyolefins have been found to be most suitable for making hollow-fiber membranes. The melt-spun approach has three key stages that occur in the following order: fiber melt extrusion, annealing, and stretching of the annealed film/fiber parallel to the spinning direction. This process method has led to commercialization of microporous materials based on high-density polyethylene (HDPE) and isotactic polypropylene (iPP). To achieve a microporous membrane by this approach, it is first necessary to develop a precursor film/hollow fiber made by the spinning extrusion process that possesses a planar-stacked lamellar semicrystalline texture. Crystallization under higher stress is thus essential, according to the Keller and Machin model,[19,20] to produce this morphology. This important and well-recognized morphological model suggests that an axial-directed stress in the melt, as controlled by the processing conditions, is essential for fibril nucleation. Accordingly, low extrusion stress during crystallization produces a twisted lamellar morphology that nucleates from a central fibril nucleus to form winding ribbon structures. It was suggested[21] that the criteria

Correspondence to: Jianli Wang (wangjl@zjut.edu.cn).
Contract grant sponsor: Zhejiang Natural Science Foundation; contract grant number: ZJNSF Y404096.

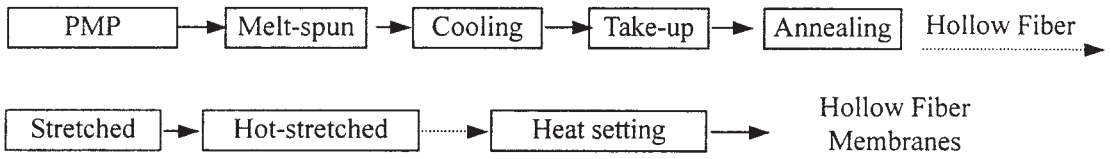

Figure 1 Flow chart of the preparation of PMP hollow-fiber membranes with MSCS.

or prerequisites that a semicrystalline polymer must fulfill to form a "quality" microporous membrane via the three-stage MSCS process are: (1) "fast" crystallization kinetics, (2) a highly planar lamellae morphology for the extruded precursor, (3) "high" orientation of the crystalline phase in the precursor, (4) proper film thickness (1 mil) and quenching rate to facilitate rapid heat transfer of the film, and (5) presence of a α_c relaxation.

One polymer of semicrystalline polymer, poly(4-methyl-1-pentene) (PMP), has shown particularly desirable gas permeation properties.[22,23] As PMP is easily processable, it is currently regarded as the best material for homogeneous membranes for gas separation.[24] The potential application of a polymer as a separation membrane depends on both the possible throughput and the purity of the product. This means that both the permeation rate for the gas that is transported more rapidly and the selectivity should be as large as possible. For a given polymer material such as PMP, to fabricate asymmetric and/or composite membranes with a thin selective layer is a suitable choice for increasing the gas permeation rate.[25–27] Matthew et al.[21] investigated a three-stage process (melt-extrusion/annealing/uniaxial stretching) to produce isotactic poly(4-methyl-1-pentene) microporous films. It is well known that hollow-fiber membranes are the most advantageous form of membranes used in the processes of separation. The mechanism of the formation of melt-spun asymmetric PMP hollow-fiber membranes has been discussed in the literature[24]; however, no information is available about characterization of hollow fibers/membranes, especially the development of the pore structure of PMP hollow fibers from asymmetric to microporous. In the present study, PMP hollow fibers/membranes were prepared by the MSCS method. Formation of the morphology of the original hollow fibers and development of the textile pores of the membranes were especially emphasized.

EXPERIMENTAL

Materials

The original hollow fibers were formed from a melt of poly(4-methyl-1-pentene) supplied by Mitsui Petrochemical Ind. (Tokyo, Japan), under the commercial name of TPX type RT-18, with a melt flow index of 26 g/10 rain. Figure 1 shows the flow chart for the preparation of PMP hollow fibers by the MSCS process. The PMP was extruded and spun to form hollow fibers on a single-screw extruder with a single-hole tube-in orifice-type spinneret (Fig. 2). The PMP hollow fibers then were stretched to a certain drawn ratio at 120°C and annealed at 180°C for desired time.

Crystallinity

DSC measurement was performed with a Perkin-Elmer DSC-7 operating at a cooling rate of 10°C/min utilizing sample weights of about 5 mg. The raw resin temperature was raised to 280°C for 10 min followed by cooling to follow crystallization. The samples were then reheated to 280°C for 15 min followed by a second crystallization. The results of both cooling scans were analogous. All DSC scans were performed under an N_2 atmosphere. Heating scans of the hollow fibers were also conducted using a heating rate of 10°C/min from room temperature to 280°C with a sample weight of approximately 5 mg. The mass fraction of crystallinity was calculated from the following mass fraction relationship

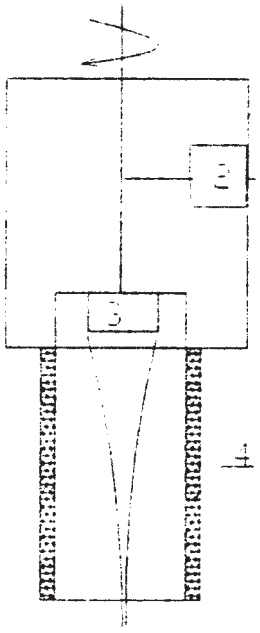

Figure 2 Subspinneret zone of extruder spinning machine: spinneret with warm keeper. (1) heating jacket; (2) polymer gear pump; (3) spinneret; (4) heat insulator; (5) hollow fiber.

TABLE I
Geometrical Sizes of the Fiber and Crystallinity with Different Take-up Speed (polymer pump: 25r/min, spun temp. 270°C)

No.	1	2	3	4	5	6
Take-up speed (m/min)	150	200	226	250	300	350
D_i (μm)	272	265	267	260	240	230
Thickness (μm)	60	50	48	46	45	45
X_c (%)	33.26	33.52	33.42	33.30	33.51	—

$$X_c(\%) = \Delta H / \Delta H^0 \times 100$$

where ΔH_f is the measured heat of fusion per gram from the area under the melting endotherm and ΔH_f° is the enthalpy of fusion per gram of a 100% crystalline sample. For i-PMP, several values ΔH_f° have been reported, ranging from 65.4 to 118.9 J/g.[28] A ΔH_f° value of 65.4 J/g was chosen and used throughout this study for no other reason than to have a consistent value for calculating the crystallinity. To determine the crystallinity, the area under the melting endotherm for a sample was calculated using the standard supplied Perkin-Elmer software at a heating rate of 10°C/min.

Mechanical property

The stress–strain behavior of the hollow fibers was tested using a XL-250A tensile testing machine (Guangzhou Test Instrument Factory).

Fiber morphology

The morphology of the samples was examined using a Hitachi S-570 scanning electron microscopy (SEM) at an accelerating voltage of 20 kV. The surfaces of the samples were coated with a thin film of gold to prevent charging prior to the SEM examinations.

Characterization of membrane

Porosity

The porosity (P) of the hollow-fiber membrane was determined using a density method. A certain length of hollow fiber was weighed. The outer and inner diameters of the hollow fiber were determined by averaging the diameters of 10 samples measured using a microscope. Then the density (ρ) of the hollow fiber was defined as

$$\rho = \frac{W}{\pi(R^2 - r^2)l}$$

where W is the weight of the hollow fiber, R and r are the outer and inner diameters, respectively, and l is the length of the hollow fiber.

Thus, the porosity of the hollow-fiber membrane was defined as

$$P(\%) = (\rho_0 - \rho_1)/\rho_0 \times 100$$

where ρ_0 and ρ_1 are the density of the hollow fiber before and after straining, respectively.

Gas permeation

About 10 hollow-fiber membranes were bundled in a U shape, and their open ends were fastened with epoxy resin to fabricate a module. Every hollow-fiber membrane was about 10 cm in length. Then, a gas (gas, oxygen, or carbon dioxide) pressure of 0.1 MPa was applied to the inside of the hollow-fiber membrane at 25°C, and the amount of nitrogen that permeated through the membrane was determined. The gas permeation (J) was calculated according to the following equation

$$J = \frac{V_{\text{gas}}}{A \times P \times t}$$

where V_{gas} is the gas volume that permeates through the membrane, A is the membrane area calculated on the basis of the inner diameter of the hollow-fiber membrane, P is the gas pressure difference between the upside and downside of the membrane, and t is the time when gas permeates through the membrane. The gas separation selectivity/factor, α_j^i, was determined by J_i/J_j where i and j are CO_2, O_2, or N_2.

RESULTS AND DISCUSSION

Effect of extrusion and annealing conditions on hollow fibers

As described in the literatures, the melt-spun temperature of the spinneret, extrude velocity, surrounding (cooling) temperature, take-up speed, and spinneret size greatly influenced the final morphologies of the spun hollow fibers. According to the calculations, the polyolefin hollow fiber was formed at a spinning distance almost within 0.5 m.[29] This indicates that the well-controlled temperature in this area was the most

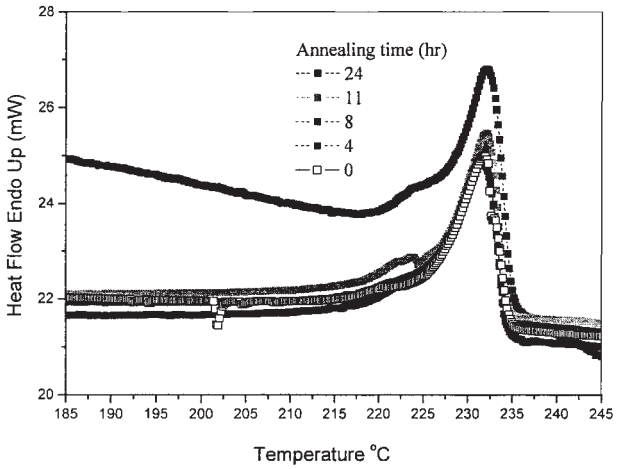

Figure 3 DSC analysis of PMP hollow fibers annealed for different times at 185°C.

important factor in achieving a high-stress field in the melt, which was favorable to a macromolecular chain orientation.

Take-up speed

PMP hollow fibers with different draw ratios were prepared by changing the take-up speed while the extrusion rate of the melt polymer solution remained constant. As shown in Table I, the inner diameter and thickness of the hollow fiber were reduced as take-up speed increased from 150 to 350 m/min. A previous study reported that the stretching stress of melts polymer increased with draw ratio, benefiting linear nucleation, molecular chain orientation, and lamellae formation. However, in the present study, processing conditions such as take-up speed had little influence on the crystallinity (X_c) of the original fibers (see Table I). Almost all X_c values were slightly higher than 33%, which was less than the X_c (49.2%) of the PMP pellet. This may have been a result of the high melt-spun temperature and the quick freezing of the polymer melt.

Annealing condition (temperature and period)

After the hollow fibers have been spun from the spinneret and taken up, they should be annealed below the melting point of PMP to increase the X_c of the hollow fiber. Then the micropores can be more readily formed in the fiber wall during the straining process. In the annealing process, annealing temperature and time are the two key factors influencing the structure and properties of the hollow-fiber membranes. After the hollow fibers were extruded from the spinneret, they underwent stress crystallization rapidly, and hence row-nucleated crystals formed. However, the process was so short that there were many molecular chains that aligned irregularly in lamellae. Thus, many defects existed after the hollow fibers were taken up. Upon being annealed under the proper conditions, these unstable defects would reorder to form more perfect structures. The result was a reduction in defects and the formation of more stable crystals. Moreover, the density of the hollow fibers showed some increase because of higher crystallinity, as reported by Kim et al.[7] for the preparation of polypropylene hollow-fiber membranes.

DSC analysis of the original hollow fibers showed that the melt peak of the fibers occurred at about 230°C and that the melt scale ranged from 210°C to 235°C (see Fig. 3). Thus, a temperature of 185°C was selected as the annealing temperature, which was 25°C below the temperature of the onset of the melt of the fiber.

Table II shows the effect of annealing time on the X_c and melt peak of the annealed hollow fibers at 185°C for a certain time. Crystallinity increased from 33% to 47% with increasing annealing time and finally almost equaled that of the original resin pellet. But it seemed that this polymer chain perfection took much longer than that reported for polypropylene and polyethylene hollow fibers in other studies. Nearly 12 h was needed to achieve crystallization equilibrium. That was quite different from the situation of PP and PE hollow fibers, for which annealing times of 2 and 1 h, respectively,[30,31] were sufficient to allow polymer chain reorder and touch balance, respectively. A possible explanation for this is that the polymer with more soft molecular chains needed less annealing time regardless of annealing temperature. Clearly, the melt peaks of the thermo-treated fibers moved higher as annealing time was prolonged (see Fig. 3 and Table II).

The typical force–strain curves of the original and annealed hollow fibers are shown in Figure 4. It can be

TABLE II
Effect of Annealing Time at 185°C on Crystallinity and Melting Peak of PMP Hollow Fibers (spun temperature 270°C; take-up speed, 300 m/min)

Sample	1	2	3	4	5	6
Annealing time (h)	0	1	4	8	12	24
X_c (%)	33.0	35.0	42.7	43.8	46.8	47.0
Peak T_m (°C)	231.0	231.9	231.8	232.0	232.1	232.2

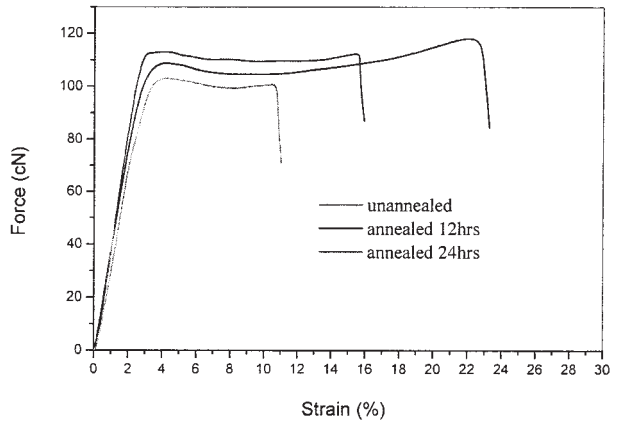

Figure 4 Force–strain curves of PMP hollow fibers (fiber length: 250 mm; stretching velocity: 500 mm/min at 20°C).

seen that the broken strain of the original PMP fiber was about 10% and that the annealed one (12 and 24 h) increased less than 25%, however. The stretching behavior of this annealed PMP hollow fiber did not show any apparent so-called hard elasticity unlike with PP or PE hollow fibers prepared by the MSCS method and annealed.

Morphologies of hollow fibers

Many crystal spheres, which ranged in size from about 1 to 2 μm, could be observed in the SEM picture of the outer surface of the hollow fiber [Fig. 5(b)]. Also, this original PMP hollow fiber had quite different inner and outer surfaces (see Fig. 5).

The temperature difference between inner and outer surfaces can be explained and described by Figure 6. As the polymer melt-spun from the spinneret, the outer surface of the hollow fiber contacted directly with the cooling air and solidified more quickly than did the polymer melt radical along its radius. Furthermore, the inner surface contacted with warm nitrogen, which was heated by the spinneret. The relatively low strain on the hollow-tube polymer melt was more beneficial to spherical crystallization. In fact, whether solidification of the polymer melt results in the formation of more spherical crystals or more lamellae under spinning and drawn stress is a competitive process.

After annealing, the number of "spherulites" on the outer surfaces of the hollow fibers decreased, and traces along the extruded direction could be found [see Fig. 5(d)]. This means that more crystals formed and that part of the spherical crystallization changed into the more stable lamellae state.

In addition to the already-mentioned observed difference between the outer and inner surfaces of the original and annealed hollow fibers, additional contrasts in morphology along the radius of the fiber cross section also were defined (see Fig. 7). From the inside

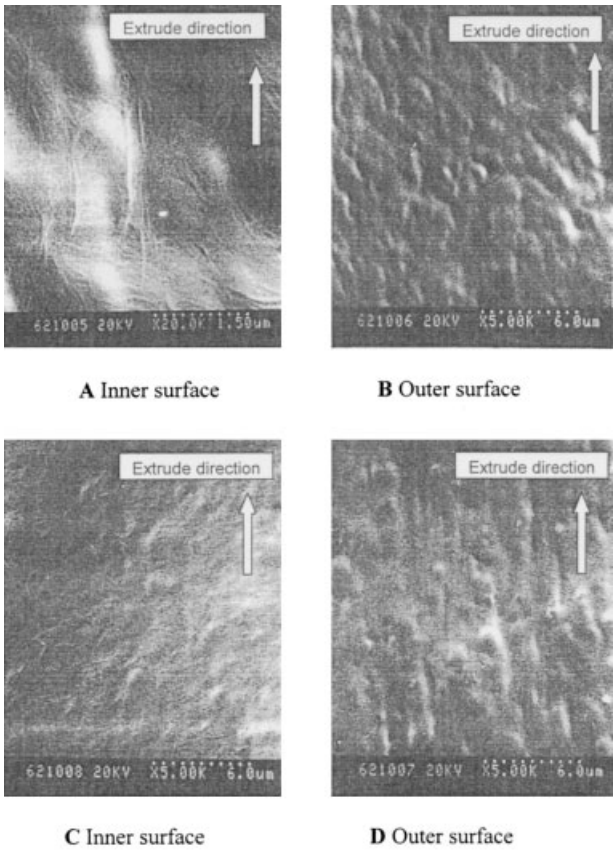

Figure 5 Scanning electronic microscope (SEM) photos of (a)/(b) original hollow fiber and (c)/(d) annealed hollow fiber (spinning temperature 270°C, mass extruding 15 g/m, take-up speed 200 m/min).

to the outside of the hollow fibers, there were three kinds of macromolecular coagulation; the interlayers especially showed a regular piled structure, which indicated the presence of more perfect lamellae. We named these layers (see Fig. 8), going from the inside boundary to outer side of the section, the loose lamella layer, the lamella layer, and the spherical crystal layer. The thicknesses of these layers, shown in Figure 7, were approximately 9, 30, and 6 μm, respectively, evaluated from the cross section of the resulting hollow fiber. The morphology of this hollow-fiber cross section depended on variations in the cooling speed and the stress field along the fiber section. This three-

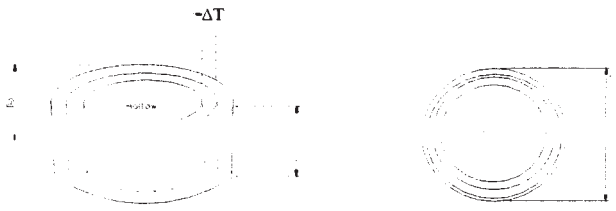

Figure 6 Schematic of temperature difference along the radial of hollow fiber.

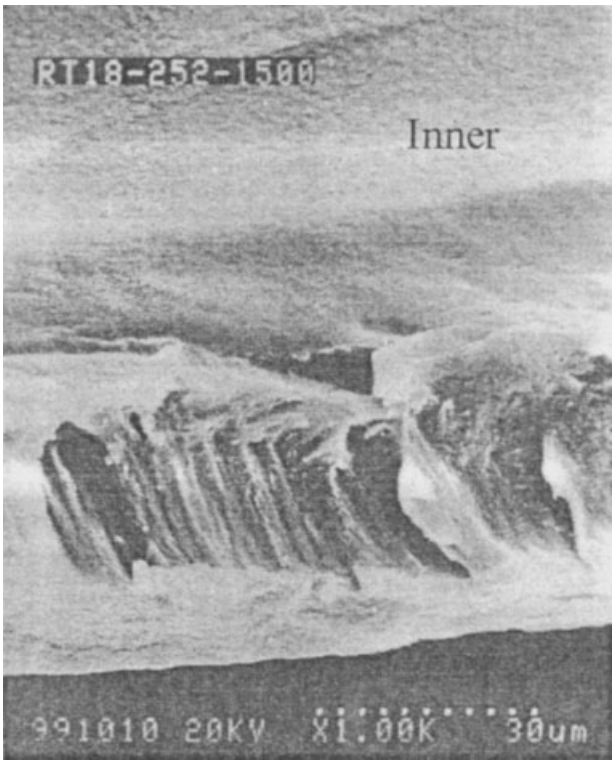

Figure 7 SEM photo of the section of unannealed PMP hollow fiber (spinning temperature 260°C, take-up speed 300 m/min).

layer model can be used to explain qualitatively the macromorphology of PMP hollow fibers formed in the spinning and take-up processes.

Effect of annealing and stretching conditions on hollow-fiber membranes

Effect of annealing time

The annealed hollow fibers were further stretched to form hollow-fiber membranes with a certain stretching ratio. The influence of annealing time on the gas permeation rate, J, and the separation factor, α, of the resulting membrane is shown in Figure 9. The oxygen permeation rate, J_{O_2}, of the final membrane (stretching ratio, 120%) increased slightly from 1.0×10^{-6} to 1.28×10^{-6} cm^3 cm^{-2} s^{-1} cmHg^{-1}, and the corresponding α_{O_2/N_2} was 3.7, 3.3, and 3.2, with a thermo-treatment time of 2, 10, and 60 min, respectively. That these stretched hollow fibers possessed gas separation ability indicated there was a dense polymer layer that took action on gas selectivity. The gas permeation rate, moreover, increased dramatically, finally, to 2.0×10^{-4} cm^3 cm^{-2} s^{-1} cm as annealing time increased from 300 to 1000 min. This implied that an increasing number of pores in the membranes and defects in the dense layer were formed as the hollow fibers were stretched.

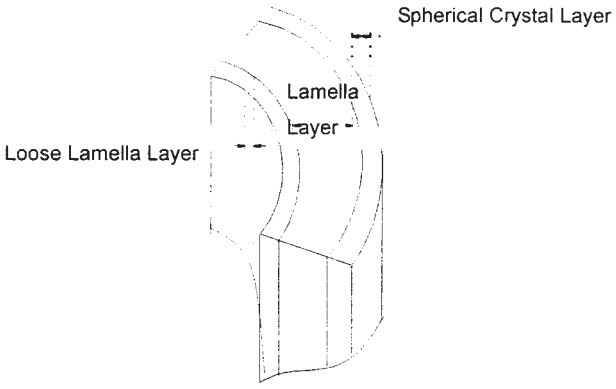

Figure 8 Model of the section morphology of PMP hollow fiber. The section is composed of outer surface and three layers: a loose lamella layer, lamella layer, and a spherical crystal layer.

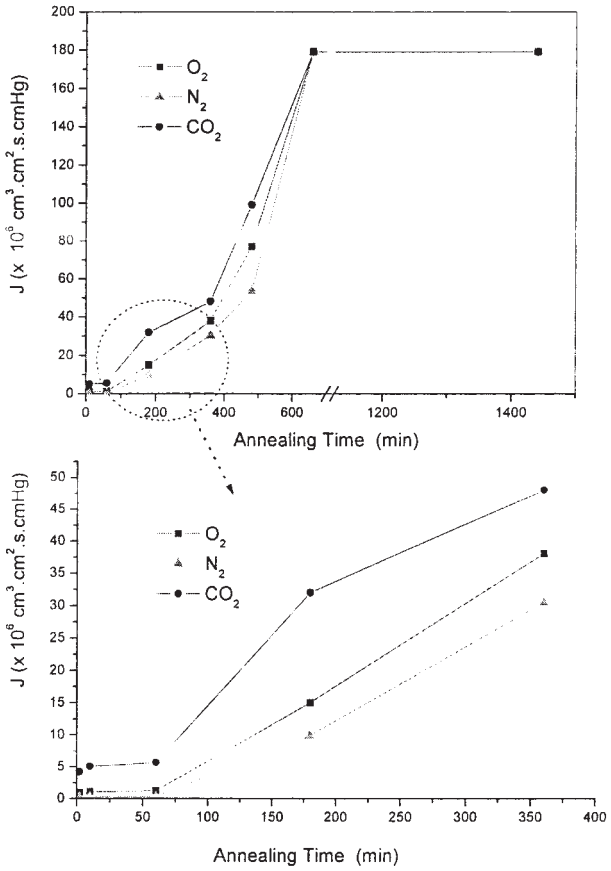

Figure 9 Gas permeation properties of PMP hollow-fiber membranes with different annealing times (spinneret temperature 270°C, polymer extruding 15 g/min, take-up speed 300 m/min, stretching ratio 120%).

Effect of stretching ratio on properties of membranes

To obtain PMP hollow-fiber membranes that had a greater gas permeation rate and higher separation selectivity, hollow fibers (annealed for 1 h) were

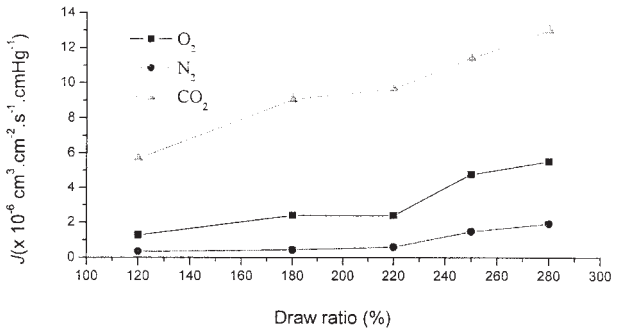

Figure 10 Relationship between gas permeation and stretching ratio (spinning temperature 270°C, take-up speed 300 m/min, annealing time 60 min).

stretched under different stretching ratios. Figures 10 and 11 display the effects of the stretching ratio on the gas separation properties of PMP hollow-fiber membranes. J_{O_2} increased from 1.28×10^{-6} to 4.7×10^{-6} $cm^3\ cm^{-2}\ s^{-1}\ cmHg^{-1}$, J_{N_2} increased from 0.34×10^{-6} to 1.48×10^{-6} $cm^3\ cm^{-2}\ s^{-1}\ cmHg^{-1}$, and J_{CO_2} increased from 5.67×10^{-6} to 1.14×10^{-5} $cm^3\ cm^{-2}\ s^{-1}$ $cmHg^{-1}$. Meanwhile, the selectivity factor of the membranes decreased and $\alpha_{N_2}^{O_2}$ decreased from 16 to 6.4. This means that the selective layer became thinner because of the plastic deformation of the skin polymer along the stretching direction. Inevitably, there were more and more defects, which induced the decrease in selectivity that appeared during this process.

The morphologies of membranes modified with different stretching ratios are shown in Figure 12. Some micropores appeared on the inner surface of sample **A** [stretching ratio is 120%, see Fig. 12(a)], and the section of **A** showed a sandwich structure [see Fig. 12(a)]. There were, however, no pores on the outer surface of the same hollow-fiber membrane. This morphology can be explained by the so-called sandwich model, described in previous structural descriptions of hollow fibers.

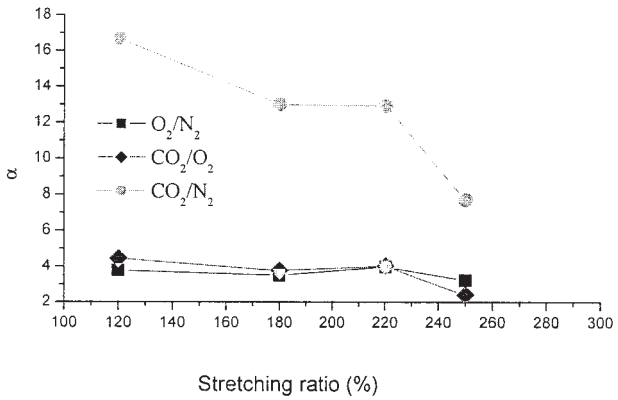

Figure 11 Effect of stretching ratio on the separation factors.

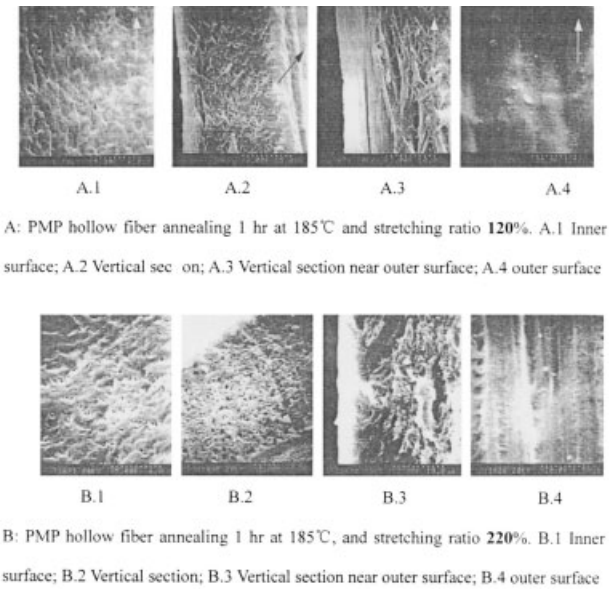

Figure 12 SEM photos of PMP hollow-fiber membranes with stretching ratios of (a) 120% and (b) 220% (origin hollow fiber: spun temperature 270°C, take-up speed: 250 m/min, annealed 1 h at 185°C).

Sample B was prepared with a larger stretching ratio [220%, see Fig. 12(b)]. It can be seen that when the hollow fiber was stretched many more pores appeared on the inner surface of the membrane than on that of sample A [Fig. 12(b)1]. However, the pore distribution across the section was not uniform, especially at the outside boundary. The SEM photos of the outer and inner surfaces also show this [Fig. 12(b)1,4]. On the outer surface of the fiber only parallel trails, which were caused by stretching, can be observed.

Table III shows the variation in the porosity of the PMP hollow-fiber membranes. Using the same stretching ratio, the membrane prepared from the fiber with a longer annealing time had larger porosity. For instance, as shown in Table III, the porosities of PMP hollow-fiber membranes prepared by stretching (ratio 120%) hollow fiber annealed for 1 and 24 h were 10% and 27%, respectively. Simultaneously, the diameters of the stretched fibers decreased with the stretching

TABLE III
Porosity of PMP Hollow-Fiber Membranes

	Stretching ratio (%)			
P_r (%)	120	180	200	250
Annealing time (h)				
1	10.6	—	—	—
4	17.1	—	—	—
8	19.5	—	40.5	—
11	24.0	—	—	—
24	26.7	38.3	42.2	48

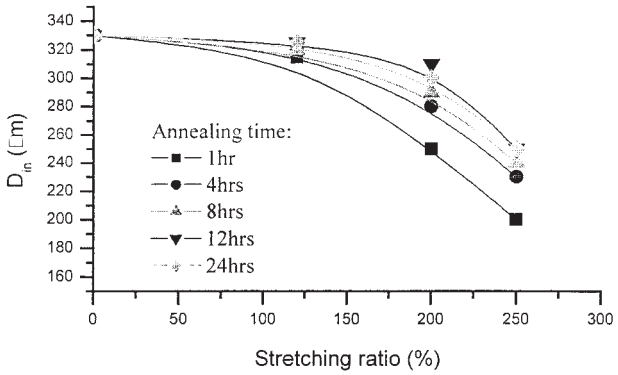

Figure 13 Outer diameters of PMP hollow-fiber membrane changed with stretching ratios.

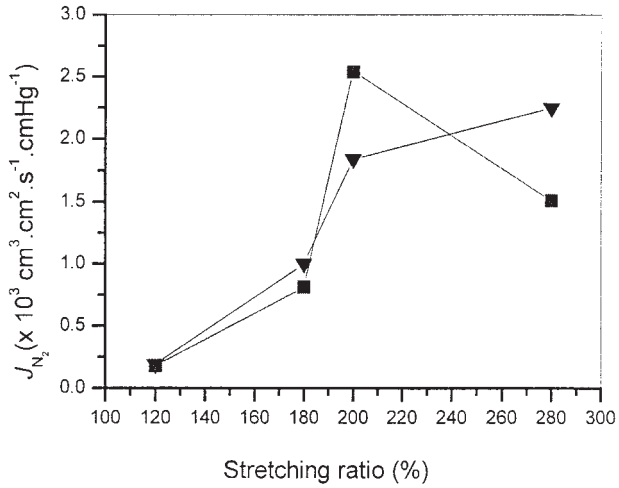

Figure 14 Relationship between gas permeation and stretching ratio (spun temperature 270°C, take-up speed 300 m/min, —▼— annealing time of 24 h, —■— annealing time of 12 h, all at 185°C).

ratio, with the diameter of the fiber with less annealing time decreasing more sharply (see Fig. 13). It is believed that plastic deformation of the polymer matrix will induce a large deformation, whereas hard elastic deformation induces less change in the diameter of hollow fibers. It was also found that the differences in deformation between PMP hollow fibers and other annealed polyolefin hollow fibers, such as hard elastic polyethylene and polypropylene, were quite apparent.

The dense thickness of hollow-fiber membranes can be evaluated by the formula

$$P = J \times x$$

where $P_{O_2}^{25°C} = 2.0 \times 10^{-9}$ cm^3 cm cm^2 s cmHg^{-1}, the permeation coefficient of oxygen, and $J_{O_2}^{25°C}$ were used to calculated the thickness, x. The results calculated according to the data in Figure 10 are listed in Table IV. On the basis of the above analysis, it can be concluded that annealing time almost dominated the gas permeation properties of hollow-fiber membranes fabricated by poststretching. The hollow-fiber membrane prepared under conditions of low stretching ratio and short annealing time (less than 3 h) had good gas separation selectivity. In contrast, the gas selectivity of the membrane drawn from original fibers annealed 4–6 h was reduced dramatically with an increase in the stretching ratio. The membrane stretched by hollow fibers annealed 24 h (in Fig. 9) lost its ability to separate gas and had a nitrogen permeation rate of 10^{-4} cm^3 cm^{-2} s^{-1} cmHg^{-1}, even with a low stretching ratio (120%). So it can be concluded the annealing time and stretching ratio are the key factors that influence the gas permeation performance of the resulting membrane. Figure 14 shows gas permeation of a stretched membrane derived from hollow fibers with relatively longer annealing times of 12 and 24 h, respectively. As the stretching ratio increased from 120% to 280%, the nitrogen permeation rate of the stretched fiber (annealed 24 h) increased from 1.79 × 10^{-4} to 2.25 times; 10^{-3} cm^3 cm^{-2} s^{-1} cmHg^{-1} and that of the fiber (annealed 12 h) increased from 1.79 × 10^{-4} to 1.51 × 10^{-3} cm^3 cm^{-2} s^{-1} cmHg^{-1}.

TABLE IV
Calculated Effective Thickness of PMP Hollow Fibers with Different Stretching Ratios

Stretching ratio (%)	120	180	220	280
J_{O_2} (× 10^6 m^3 cm^{-2} s^{-1} cm Hg)$^{-1}$	1.28	2.0	4.1	4.7
x (μm)	15.6	10.0	4.9	4.3

Morphologies of PMP hollow-fiber membranes

The morphology of PMP hollow-fiber membranes fabricated under various conditions was examined by SEM in order to be able to directly observe the fine structure. Figure 15(a–h) shows the SEM photos of the inner and outer surfaces of the series of membranes whose stretching ratio was 200% and whose fiber annealing times were 1, 4, 8, 12, and 14 h, respectively. It can be seen that a longer annealing time resulted in more micropores on the surfaces of the hollow fibers, which was consistent with the variation in the gas permeation rate and separation selectivity of the respective membranes. It was clearly shown in the present study that PMP hollow fibers developed gradually from asymmetric gas separation membranes into microporous membranes when annealing time was longer than 11 h [shown in Fig. 15(c–h)]. There is no doubt about the perfect annealing of the lamella structure of the original fiber, which was the network backbone of the porous membrane. This perfection not

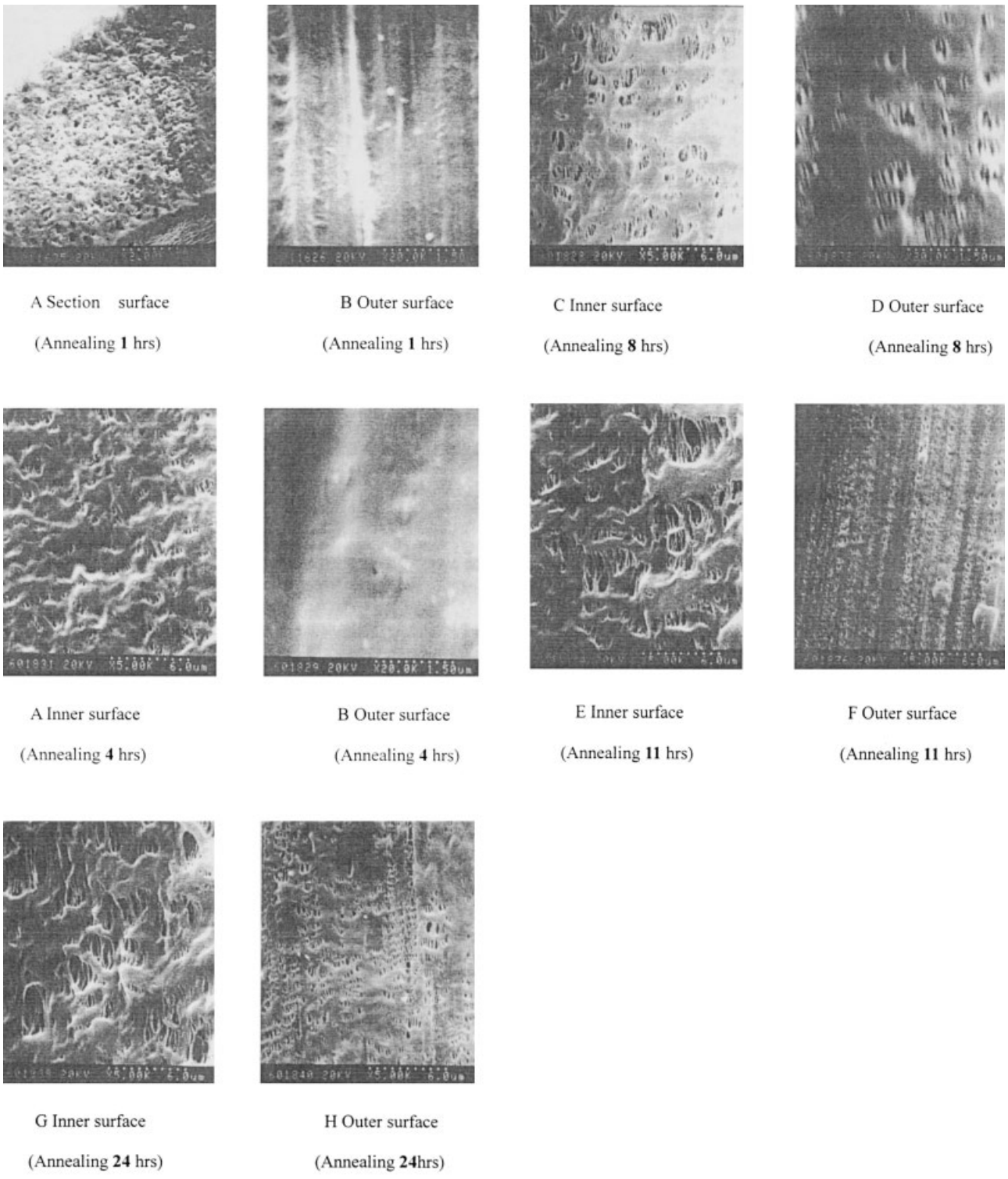

Figure 15 SEM photos of PMP hollow-fiber membranes at different annealing times (spinneret temperature 270°C, take-up speed: 300 m/min, stretching ratio 200%).

only increased the number of lamellae in the fiber, but also induced spherulite transfer into lamellae in a strain annealing state. The final results were that the lamella layer along the section of the fiber increased and the thickness of the outside spherulite layer decreased, so that the longer annealed fiber was drawn relatively easily in order to expose the deeper inner textile structure [as shown in Fig. 15(f,h)]. These pho-

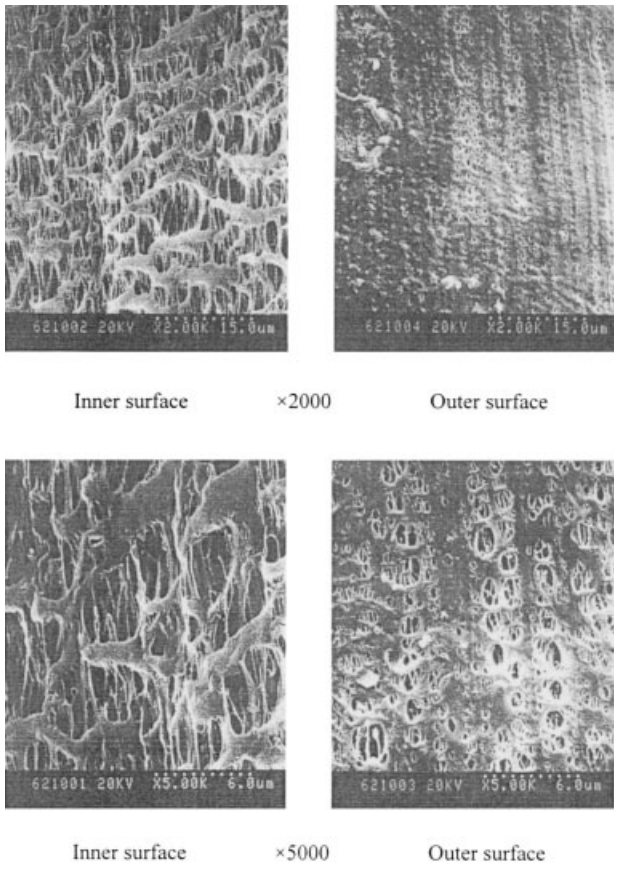

Figure 16 SEM photos of PMP hollow-fiber membranes annealing for 24 h at 185°C, with a take-up speed of 300 m/min and a stretching ratio of 280%.

tos clearly show the surface layer trail along the drawn direction. Although the annealing time was 24 h, the outer surface displayed the morphology of a typical microporous membrane manufactured by the melt-spun and cold-stretching method. Synchronously, the inner-surface layer clearly developed high porosity becoming large pore networks. The average pore size in the inner surface was almost 10 times that of the inner surface estimated from the photos.

The surface morphology of the membrane with an annealing time of 24 h and a stretching ratio of 280% is shown in Figure 16. Compared with the membrane with an annealing time of 24 h and a stretching ratio of 200% [Fig. 15(g–h)], the network was more regular and the pore sizes were larger. It was clearly seen that the outer surface of the resulting membrane was composed of skin and microfiber, which formed slitlike micropores. In this situation, the texture of the outer surface was similar to that of PP and PE hollow-fiber membranes.

Water permeation

The water permeation of a series of hollow-fiber membranes prepared in various conditions (annealing time and stretching ratio) was tested, and the results are listed in Table V. First, the permeation performance of the original membranes was tested to confirm that no water permeated the membranes. The results indicated that PMP was a good hydrophobic material. After immersion in alcohol, the membranes prepared from hollow fibers with a longer annealing time and a larger stretching ratio were found to have much larger water flux, results consistent with those for the gas permeation measurement.

CONCLUSIONS

Melt-spun PMP hollow fibers using air as a cooling medium showed an apparently asymmetric structure. Take-up speed directly influenced diameter size but had little effect on the crystallinity of the hollow fibers. More than 12 h of annealing at 180°C was needed to achieve balanced crystallization. A three-layer model was used to describe the morphology and formation of asymmetric structure of PMP hollow fibers. Various PMP hollow-fiber membranes were prepared by the MSCS method. Posttreatment conditions, especially annealing time and stretching ratio, were investigated. The results revealed that the original PMP hollow fibers were easily modified to become hollow-fiber membranes. The annealing time of the hollow fibers and the stretching ratio were the key factors that influenced the physical structure and gas separation properties of the stretched membrane. The original fibers that had been annealed for less than 4 h could be easily stretched into an asymmetric membrane that had the ability to separate the gas pairs oxygen/nitrogen and oxygen/carbon dioxide. The hollow-fiber membrane had a special radial structure: a large-pore layer on the inner surface, a regular lamella network layer in the middle structure, and a relatively compact layer on the outer surface. Water flux tests were carried out with the resulting microporous PMP membranes with and without soaking in ethanol.

The authors thank SRF for ROCS and SEM.

TABLE V
Pure Water Flux Measurement of PMP Hollow-Fiber Membranes, Dead-End Filtration under 0.1 Mpa All Membranes Made Hydrophilic with Alcohol

Water flux (L m^{-2} hr^{-1} kg^{-1})	Stretching ratio (%)			
	120	180	200	250
Annealing time (h)				
4	None	None	None	None
8	None	None	None	None
11	None	0.8	6.9	5.2
24	0.3	1.1	2.3	6.3

References

1. Lloyd, D. R.; Kinzer, K. E.; Tseng, H. S. J Membr Sci 1990, 52, 239.
2. Chung, T. C.; Lee, S. H. J Appl Polym Sci 1997, 64, 5675.
3. Matsuyama, H.; Yuasa, M.; Kitamura, Y.; Teramoto, M.; Lloyd, D. R. J Membr Sci 2000, 179, 91.
4. Matsuyama, H.; Maki, T.; Teramoto, M.; Asano, K.; Lloyd, D. R.; Kinzer, K. E.; Tseng, H. S. J Membr Sci 2002, 204, 323.
5. Kamada, K.; Minami, S.; Toshida, K. U.S. Pat. 4,055,696 (1977).
6. Shino, M.; Yamamoto, T.; Fukunage, O.; Yamamori, H. U.S. Pat. 4,530,809 (1995).
7. Kim, J. J.; Jang, T. S.; Kwon, Y.D.; Kim, U. Y.; Kim, S. S. J Membr Sci 1994, 93, 209.
8. Shen, L.-Q.; Xu, Z.-K.; Xu, Y.-Y. J Appl Polym Sci 2002, 84, 203.
9. Nago. S., Mizutani. Y. J Appl Polym Sci 1998, 68, 1543.
10. Bierenbaum, H. S.; Isaacson, R. B.; Druin, M. L.; Plovan, S. G. Ind Eng Chem Prod Res. Dev 1974, 13, 2.
11. Callahan, R. AICHE Symp 1988, 54, 84.
12. Sarada, T.; Sawyer, L. C.; Ostler, M. I. J Membr Sci 1983, 15, 97.
13. Chen, R. T.; Saw, C. K.; Jamieson, M. G.; Aversa, T. R.; Callahan, R. W. J Appl Polym Sci 1994, 53, 471.
14. Wang, J. L.; Xu, Y. Y.; Xu, Z. K.; Xu, H. Water Sci Technol: Water Supply 2000, 5–6, 185.
15. Williams, J. L.; Gunther, H.; Peterlin, A. U.S. Pat. 89,516 (1974).
16. Soehngen, J.; Ostrander, K. U.S. Pat. 4,257,997 (1981).
17. Mizutani, Y.; Nakamura, S.; Kaneko, S.; Okamura, K. Ind Eng Chem Res 1993, 32, 221.
18. Graessley, W. W. J Chem Phys 1967, 47, 1942.
19. Keller, A.; Machin, M. J Macromol Sci Phys 1967, B1(1), 153.
20. Keller, A.; Kolnaar, J. W. H. Progr Colloid Polym Sci 1993, 92, 81.
21. Matthew B.; Johnson, G.; Wilkes, L. J Appl Polym Sci 2002, 84, 1076.
22. Lai, L. Y.; Shieh, J. J.; Shyn, S. S. J Appl Polym Sci 1989, 37, 2907.
23. Jyampolski, J. P.; Volkov, V. V. J Membrane Sci 1991, 64, 191.
24. Schmldt, K. T.; Andrzej, W. J Membr Sci 1997, 137, 55.
25. Lai, J. Y.; Wu, G. J.; Shyu, S. S. J Appl Polym Sci 1987, 34, 559.
26. Pusch, W.; Walch, A. J Membr Sci 1982, 10, 325.
27. Strathmann, H. J Membr Sci 1981, 9, 121.
28. Karasz, F. E.; Bair, H. E.; O'Reilly, J. M. Polymer 1967, 8, 547.
29. Wang, J. L. Doctoral Dissertation, Zhejiang University, 2001.
30. Xie, B. M. Master's Dissertation, Zhejiang University, 1995.
31. Xu, C. H. Master's Dissertation, Zhejiang University, 1996.